Applied Surface Science 256 (2010) 6543–6549

Contents lists available at ScienceDirect

Applied Surface Science

journal homepage: www.elsevier.com/locate/apsusc

One step synthesis of vertically aligned ZnO nanowire arrays with tunable length

Gang Meng[a,b], Xiaodong Fang[a,b,*], Weiwei Dong[a,b], Ruhua Tao[a,b], Yiping Zhao[a], Zanhong Deng[a], Shu Zhou[a], Jingzhen Shao[a], Liang Li[c]

[a] Anhui Institute of Optics and Fine Mechanics, Chinese Academy of Sciences, Hefei 230031, China
[b] Key Laboratory of New Thin Film Solar Cells, Chinese Academy of Sciences, Hefei 230031, China
[c] Key Laboratory of Materials Physics, Institute of Solid State Physics, Chinese Academy of Sciences, Hefei 230031, China

ARTICLE INFO

Article history:
Received 1 December 2009
Received in revised form 2 April 2010
Accepted 14 April 2010
Available online 21 April 2010

Keywords:
ZnO nanowire arrays
Vapor phase transport
Length tuning

ABSTRACT

Length control of ZnO nanowire arrays is a valuable concern for both fundamental research and future device application. In this article, vertically aligned ZnO nanowire arrays were synthesized by a seed layer catalyzed vapor phase transport method in a single experiment cycle. The length of these nanowire arrays exhibits a quasi-continuous evolution. It was found that the type and flow rate of carrier gas have a significant influence on the length modulation of ZnO arrays along the tube. A feasible route to tune the length of ZnO nanowire arrays from several micrometers to nearly 100 μm could be achieved by adjusting proper deposition position and carrier gas.

1. Introduction

One-dimensional (1D) zinc oxide (ZnO) has received persistent and particular interest in the past decade, because of its superior performance on optoelectronic devices [1], gas sensing [2], solar cells [3], photocatalysis [4], and biocompatibility [5].

There have been a wide variety of 1D ZnO nanostructures, including nanowires, nanorods, nanonails, nanopencils, nanotubes, and so on [6–10]. Among these unique structures, vertically aligned nanowire arrays with the same crystal orientation, similar diameter, uniform length, and large density, are quite critical for device applications, as they can enhance the performance of the nanodevices remarkably. Well-aligned 1D ZnO arrays show excellent performance in a flat panel display [11], gas sensors [12], nanolasers [13], photonic band gap crystals [14], piezoelectric antenna arrays, and nanoelectromechanical systems (NEMS) [15].

Controlled growth of nanowire arrays with desired size (including diameter and length) and density is necessary for functional nanodevices assembly. Among numerous approaches to synthesize ZnO nanowire arrays, vapor phase transport (VPT) method based either vapor–liquid–solid (VLS) or vapor–solid (VS) process is widely used because of simple apparatus requirement and controllable synthesis. Metal catalyst is used in VLS synthesis process. The main drawback is that the remaining metal catalyst may cause contamination. Metal catalyst-free synthesis of vertically aligned ZnO nanowires via VS process appears to be more versatile [16–18], since Tseng et al. reported the synthesis of ZnO nanowires by using Ga doped ZnO film as seed layer [19]. And much effort has been devoted to the alignment control [20], diameter control [2] and density control [21,22] growth of ZnO nanowire arrays, but there are few reports focused on length control of ZnO nanowire arrays. Length control is a valuable concern for both fundamental research and device application. Generally the length of 1D nanostructures can be modified by adjusting the growth time [23–25]. However, tedious repetition experiments are needed, which will be a waste of time and resource.

In this paper, well-aligned ZnO nanowire arrays have been synthesized on thin ZnO buffer layer coated Si substrates via VPT, and the length of the nanowire arrays could be tuned at a large extent by adjusting the position of seed wafers in a single growth period. A simple mode based on the mass transport of reagent gaseous species along the slender quartz tube is used to illustrate the different growth rate along the axis of the small tube. The local concentration disparity of gaseous ZnO is responsible for the length variation of nanowire arrays. The effect of carrier gas on the modulation of length variation along the tube has been systematically studied. An effective and timesaving way to tune the length of ZnO nanowire arrays could be realized by our approach.

* Corresponding author at: Anhui Institute of Optics and Fine Mechanics, Chinese Academy of Science, Hefei 230031, China. Tel.: +86 551 5593508; fax: +86 551 5593527.
E-mail address: menggang@mail.ustc.edu.cn (X. Fang).

0169-4332/$ – see front matter.
doi:10.1016/j.apsusc.2010.04.045

2. Experimental

ZnO nanowires were fabricated via a VPT process carried out in a horizontal tube furnace as illustrated in our previous literatures [26,27]. Briefly, 0.3 g mixture of zinc oxide and graphite powder was loaded at the bottom of a slender and one-end sealed quartz tube. Several *c*-axis orientated ZnO seed wafers prepared by pulse laser deposition (PLD) were placed 5–25 cm away from the source material. 5 sccm air was used as carrier gas. The furnace was heated to 900 °C and kept for 30 min. Thick black–grey layers were deposited uniformly on Si substrates after the reaction completed.

Samples A1, A2, A3, A4, A5 and A6 are ZnO nanowire arrays deposited at 5, 8, 12, 15, 18 and 21 cm away from the source material respectively, when 5 sccm air was used as carrier gas. To verify our experiment model and investigate the influence of carrier gas on the length tuning of nanowire arrays, 5 sccm O_2, 20 sccm O_2, 5 sccm N_2 and 20 sccm N_2 was used as carrier gas under the same experiment conditions, respectively.

The morphologies of synthesized products were characterized by a FEI Sirion-200 field-emission scanning electron microscopy (FE-SEM). The powder X-ray diffraction (XRD) was performed on a Philips X'pert PRO diffractometer with Cu Kα (λ = 1.5418 Å). Transmission electron microscopy (TEM) and selected-area electron diffraction (SAED) analyses were performed on a JEOL 2010 high-resolution transmission electron microscope. Photoluminescence (PL) spectra were carried out by Edinburgh FLS920 fluorimeter instruments with the excitation wavelength of 325 nm at room temperature.

3. Results and discussion

3.1. Morphologies and crystal structure characterization

The SEM image of ZnO seed layer is shown in Fig. 1a. The film is smooth and crack-free. Irregular grains with a size of 40–100 nm are closely packed. These nanograins act as catalyst and cause the formation of transition layer at the beginning stage of growth process. The as-formed transition layer was epitaxially grown on the seed layer and provided effective nuclei sites for 1D growth of nanowires [20]. The crystallization of seed layer has a significant influence on the final products, poorly crystallized or randomly orientated seed layer would result in sparse or randomly aligned nanowire arrays [28]. XRD pattern (shown in Fig. 1b) indicates that the thin ZnO seed layer presents a preferred c-axis orientation. Only wurtzite structure (0 0 2) peak can be detected, which is necessary for the synthesis of vertically aligned ZnO nanowires.

Black–grey products can be obtained in a wide range in the long slender tube. Several positions labeled by A1–A6 have been analyzed by SEM. Fig. 2a–f shows the SEM side views of samples A1–A6. Separate nanowires as well as bundles of nanowires show good alignment. The nanowires exhibit a quasi-hexagonal flat top (the inset of Fig. 2a). The diameters of these nanowires range from 100 nm to 400 nm, whereas most of them have diameters of 200–300 nm, regardless of different transport distances and temperature regions. The diameter dispersity is due to inhomogeneous sizes of ZnO nuclei grown on the surface of the ZnO transition layer [21].

Fig. 3 shows the typical XRD result. The as-synthesized ZnO nanowire arrays show sharp (0 0 2) peak even with a weak X-ray beam intensity (15 kV, 5 mA), indicating that the ZnO nanowires are well crystallized and highly oriented with [0 0 0 1] direction normal to the substrate. XRD ω-rocking curve of (0 0 2) peak (the inset of Fig. 3) could be used to evaluate the alignment degree. Sample A4 presents a small value (~2.5°) of full width at half maximum (FWHM) of (0 0 2) peak, which implies good alignment of nanowire arrays.

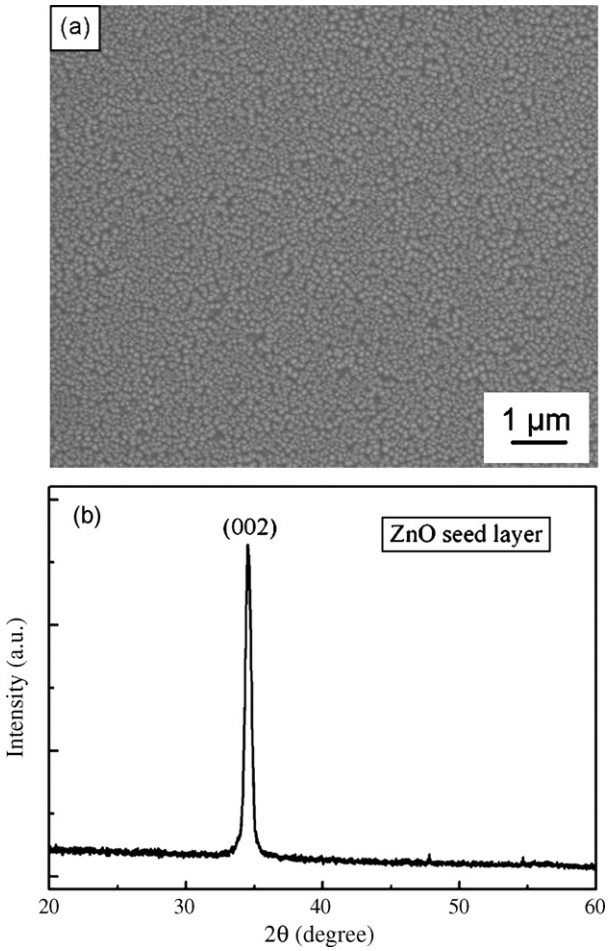

Fig. 1. (a) FE-SEM image and (b) XRD pattern of the ZnO seed layer.

SEM cross section images (Fig. 4a–f) manifest the alignment degree and length variation of ZnO nanowire arrays. It can be seen that long and straight ZnO nanowires aligned perpendicularly to the substrate except for sample A3 (Fig. 4c), which is slightly bent. The length of samples A1, A2 and A3 are 33.4 ± 2.0 μm, 60.5 ± 1.0 μm, and 81.4 ± 1.1 μm, respectively, and the value are 83.2 ± 0.7 μm, 57.3 ± 1.5 μm and 43.2 ± 1.7 μm for sample A4, A5 and A6, respectively. The length of the nanowire arrays increases firstly and then decreases with the increase of the distance away from the source materials. And the length varies at a large degree range from 33 μm to 83 μm. It is worth emphasizing that the distance between sample A1 and A6 is as long as 16 cm. Large-scale fabrications of ZnO nanowire arrays by VPT can be achieved. Samples A1–A6 were obtained by one experiment cycle: the same growth time, the same chamber pressure (pumped to ~1 Torr), slight difference in deposition temperature. The reason leading to the length dissimilarity of six samples will be analyzed in the next section. Usually the length of nanowires or nanorods can be tuned by shortening or prolonging the growth time. However, a series of experiments are necessary. It is time consuming and resource consuming. Moreover, the growth rate is usually not a constant value due to the consumption of source materials during the reaction [25]. Length control by this method is limited. Our approach is simple and effective in tuning the length of ZnO nanowire arrays.

3.2. Growth mechanism and experimental model

Since no metal catalyst is used in the experiment, the growth process does not follow VLS mechanism but VS mechanism [17].

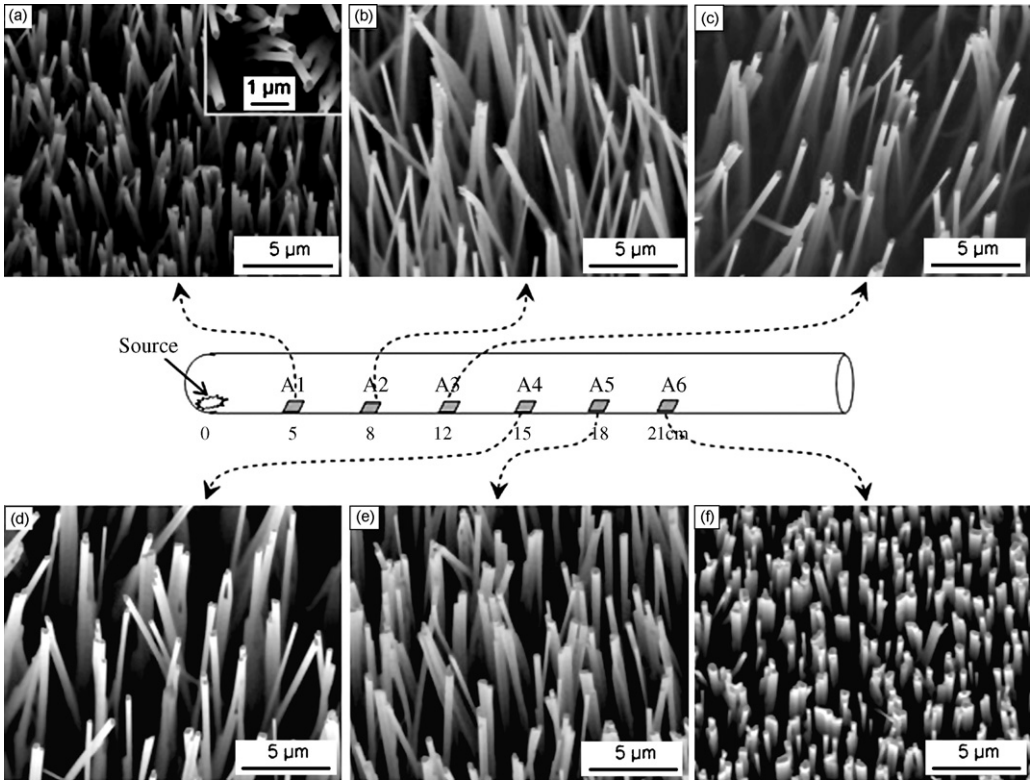

Fig. 2. The placement and the corresponding FE-SEM side view of six samples deposited under a flow rate of 5 sccm air carrier gas. (a)–(f) correspond to A1–A6, respectively. The inset of (a) shows an enlarged image.

The growth process of ZnO nanowire arrays can be summarized in three stages: vapor generation ($Zn_{(g)}$), vapor transportation (including $Zn_{(g)}$ and O_2) and vapor condensation ($ZnO_{(g)}$) [11,29].

At the first stage, once the temperature of the source materials rose to 900 °C, carbothermal reduction of ZnO occurred:

$$ZnO_{(s)} + C_{(s)} \rightarrow Zn_{(g)} + CO_{(g)}$$

$$ZnO_{(s)} + CO_{(g)} \rightarrow Zn_{(g)} + CO_{2(g)}$$

Zn vapor was released in situ from the source which was loaded at the sealed end of the small tube. Therefore, the sealed end zone was rich in $Zn_{(g)}$, and the vapor pressure of $Zn_{(g)}$ was determined by the reaction temperature [30].

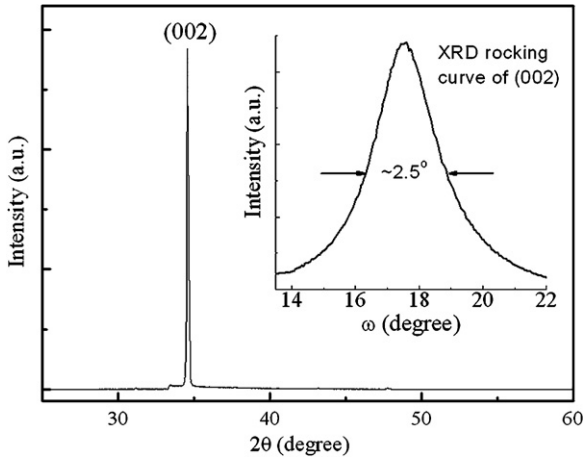

Fig. 3. Typical XRD pattern of ZnO nanowire arrays. The inset is XRD rocking curve of (0 0 2) peak (sample A4).

At the transport stage, the transport of gas species was strongly dependent on geometrical configuration of reactor. A distinctive gas transport behavior was shown when a vial [31], microchannel [32] or sealed tube [33] was used. In our experiment, a long and one-end sealed quartz tube was used to guide the reagent gas flows. The ongoing Zn vapor was confined by the inner wall of the small quartz tube and would be transported to the open end of the tube due to concentration gradient, while the other reagent gas O_2 supplied by 5 sccm air would diffuse into the sealed end. Fig. 5 gives the schematic transport process of the reagent gas species from the fundamental mass transfer perspective [34]. The opposing gas flows would confront in the small quartz tube. The oxidation reaction occurred at the overlapping region of two flows, and the local concentration of $ZnO_{(g)}$ is determined by $Zn_{(g)}$ and O_2 concentration ratio:

$$Zn_{(g)} + O_{2(g)} \rightarrow ZnO_{(g)}$$

At the third stage, gaseous ZnO molecules would fill with the tube gradually. A steady, local balanced and high vapor pressure environment was formed at the overlapping zone. 1D anisotropic growth by VS mechanism was initiated due to proper gas supersaturation range [31]:

$$ZnO_{(g)} \rightarrow ZnO_{(s)}$$

For the nanocrystal grown by vapor phase method, it is generally believed that the deposition temperature and the local gas supersaturation determine the growth rate of nanostructures [6]. In case of moderate gas supersaturation (1D growth), the relationship between the growth rate J and gas supersaturation σ, temperature T can be described by the following equation [35]:

$$J = \frac{\alpha\sigma P_0}{\sqrt{2}\pi mkT}$$

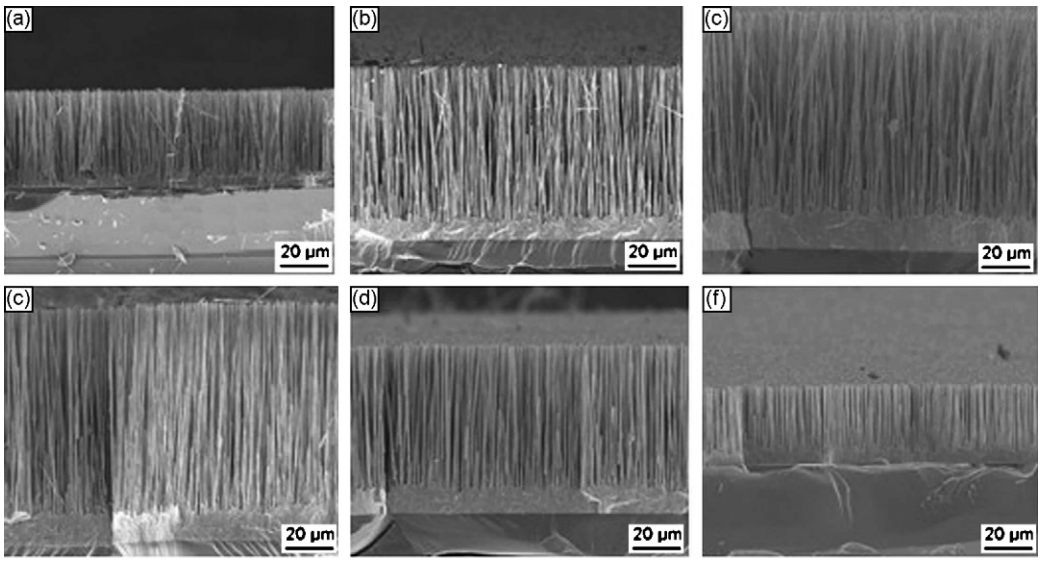

Fig. 4. (a–f) FE-SEM cross section views of nanowire arrays corresponding to samples A1–A6, respectively.

where α is the accommodation coefficient, P_0 is the equilibrium pressure, k is Boltzmann's constant and T is the absolute temperature. In our experiment, as the growth temperature variation between A1 and A6 is within 100 °C, it can be expected that the growth rate is mainly determined by vapor supersaturation, with other experimental parameters playing minor roles.

The evaluation of gas supersaturation along the tube is difficult without studying chemical reaction rate, fluid dynamics and thermodynamics variables inside the tube. A simplified reagent gas flow mode can be used to qualitatively demonstrate the differences of $ZnO_{(g)}$ concentration along the tube, by analyzing the local $Zn_{(g)}$ and O_2 concentration ratio.

$Zn_{(g)}$ was released from the source material, so the concentration was high at the sealed end. The concentration decreased with the increase of transport distance due to oxidation consumption. The narrow and semi-closed tube reactor could not provide sufficient O_2. Most of O_2 needed for the oxidization reaction was from carrier gas. Therefore, the open end zone was rich in O_2. O_2 would diffuse into the sealed end due to concentration gradient, the concentration of O_2 decreased toward upstream. The concentration of $ZnO_{(g)}$ was dependent on the concentration ratio of $Zn_{(g)}$ to O_2 seriously. A few amounts of O_2 molecules could diffuse into the sealed end of the small tube. Therefore, the concentration of $ZnO_{(g)}$ was low in the upstream. The concentration increased with the increase of transport distance, as a result of meeting more O_2 molecules. The concentration reached a peak value in the midstream of the tube due to appropriate $Zn_{(g)}$ and O_2 ratio [31], and decreased in the downstream due to severe consumption of $Zn_{(g)}$ in the midstream. The local vapor pressure of $ZnO_{(g)}$ in the midstream was higher than the upstream and downstream counterparts under a flow rate of 5 sccm air. Therefore, ZnO nanowire arrays obtained in the midstream were longer than those synthesized in the upstream and downstream.

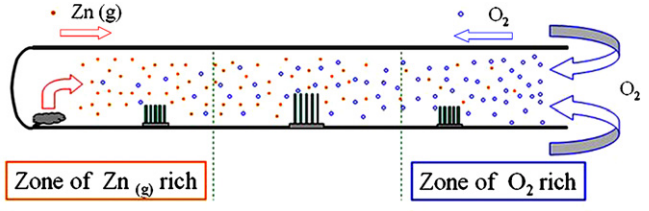

Fig. 5. The schematic illustration of reagent gas transport process in the small quartz tube. Gaseous Zn transports toward downstream, O_2 diffuses toward upstream. Gaseous ZnO was produced at the overlapping region thorough oxidization reaction.

3.3. *Effect of carrier gas on the length tuning of nanowire arrays*

The local concentration of $ZnO_{(g)}$ was dependent not only on $Zn_{(g)}$ (governed by reaction temperature), but also on the local concentration of O_2, which can be tuned by carrier gas. The following experiments were focused on the modulation of $ZnO_{(g)}$ concentration profile by varying carrier gas, keeping the other experimental parameters unchanged.

When pure O_2 with the same flow rate was introduced into the chamber, O_2 was excessive in the chamber, and sufficient O_2 could diffuse into the inner end of the tube and participate in the oxidation reaction. Then most of the Zn vapor was oxidized and consumed in the upstream of the tube soon after evaporation. Few of them could transport freely to the downstream region. The ZnO vapor concentration decreased toward downstream.

Fig. 6 shows the length variation of vertically aligned ZnO nanowire arrays deposited under pure O_2 carrier gas. 5 sccm O_2 was used as carrier gas at first. The longest nanowire arrays (Fig. 6a) with length up to 99.3 ± 1.7 μm were obtained in the upstream 6 cm away from the source, and the length attenuates quickly in the downstream. Nanowire arrays deposited at 10 cm (Fig. 6b), 15 cm (Fig. 6c) and 18 cm (Fig. 6d) are 50.0 ± 0.5 μm, 12.6 ± 0.3 μm and 1.1 ± 0.2 μm in length, respectively. The length of these nanowire arrays exhibits a tense transition from 99 μm to 1 μm in a single deposition cycle. The longest arrays are 90 times longer than the shortest arrays. The length tuning of ZnO nanowire arrays by this approach is feasible and effective. There is no longer nanowires deposition on seed wafers placed 19 cm away the source, due to the exhaustion of Zn vapor. When the flow rate of O_2 was further increased to 20 sccm, O_2 was seriously excessive compared to $Zn_{(g)}$. Most of $Zn_{(g)}$ was fully oxidized and consumed in the narrow space nearby the source material. Consequently, the $ZnO_{(g)}$ concentration in the upstream is smaller than the value under 5 sccm O_2. The length of arrays deposited at 6 cm away from the source (shown in Fig. 6e) is only 14.0 ± 0.6 μm. Nanowire arrays synthesized at 9 cm (Fig. 6f) are 1.0 ± 0.2 μm in length.

On the other hand, if pure N_2 was used as carrier gas, no O_2 was supplied from MFC. The residual O_2 in the chamber would act as reagent gas. Unfortunately, the amount of O_2 was insufficient. $Zn_{(g)}$

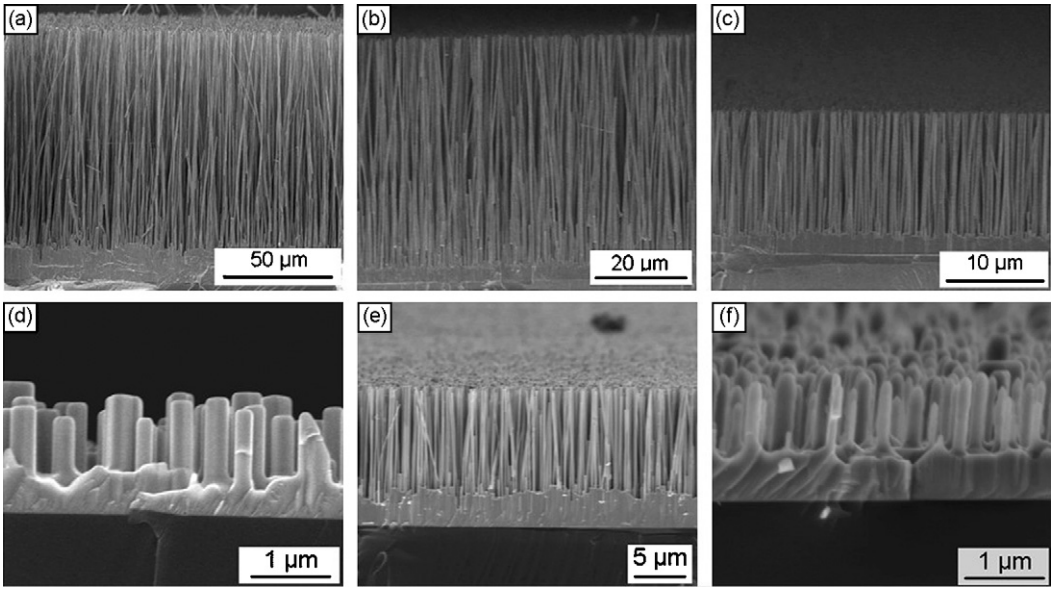

Fig. 6. FE-SEM cross section views of ZnO nanowire arrays obtained in pure O_2 carrier gas: (a)–(d) are nanowire arrays deposited at 6, 10, 15 and 18 cm away from the source respectively under a flow rate of 5 sccm O_2. (e)–(f) are nanowire arrays deposited at 6 and 9 cm respectively under 20 sccm O_2.

was partially oxidized in the transport process. The growth rate was limited as smaller amount of $ZnO_{(g)}$ was synthesized through oxidation reaction. Fig. 7a–d shows the FE-SEM cross section images of ZnO arrays fabricated under 5 sccm N_2 carrier gas. The arrays deposited at 6 cm (Fig. 7a), 10 cm (Fig. 7b), 15 cm (Fig. 7c) and 20 cm (Fig. 7d) away from the source are 3.2 ± 0.2 μm, 15.8 ± 0.6 μm, 29.8 ± 0.7 μm and 27.1 ± 1.1 μm in length, respectively. It is obvious that relatively short nanowire arrays (within 3–27 μm) can be synthesized by this approach. If the N_2 flow rate was increased further to 20 sccm, the residual O_2 was entrained by carrier gas, which resulted in the serious lack of O_2 in the chamber. $ZnO_{(g)}$ concentration was further decreased subsequently. Much shorter arrays were obtained. The arrays deposited at 15 cm (Fig. 7e) and 20 cm (Fig. 7f) are 6.5 ± 0.2 μm and 5.4 ± 0.2 μm in length, respectively.

Fig. 8 shows the correlation between length of ZnO nanowire arrays and deposition position under different carrier gases and different flow rates. Quite distinct length profiles indicate trace O_2 has a significant influence on the length (local growth rate) modulation of nanowire arrays. In the case of O_2 carrier gas, the length decreases monotonically. In the case of N_2 or air carrier gas, the length increases firstly and then decreases. Moreover, the arrays lengths can be tuned in large range under 5 sccm O_2 or air, owing to severe disparity of $ZnO_{(g)}$ concentration along the tube. Longer arrays were obtained in the area with a higher $ZnO_{(g)}$ concentration due to appropriate ratio of $Zn_{(g)}$ to O_2. Relatively short arrays could be synthesized under 5 sccm N_2, 20 sccm N_2 and 20 sccm O_2, because O_2 in the chamber is either insufficient or excessive. And the length variations along the tube are slow in these cases. Fig. 8 is instructive that ZnO nanowire arrays with arbitrary length (from ~1 to 100 μm) are expected to be synthesized by choosing proper carrier gas and adjusting the deposition position.

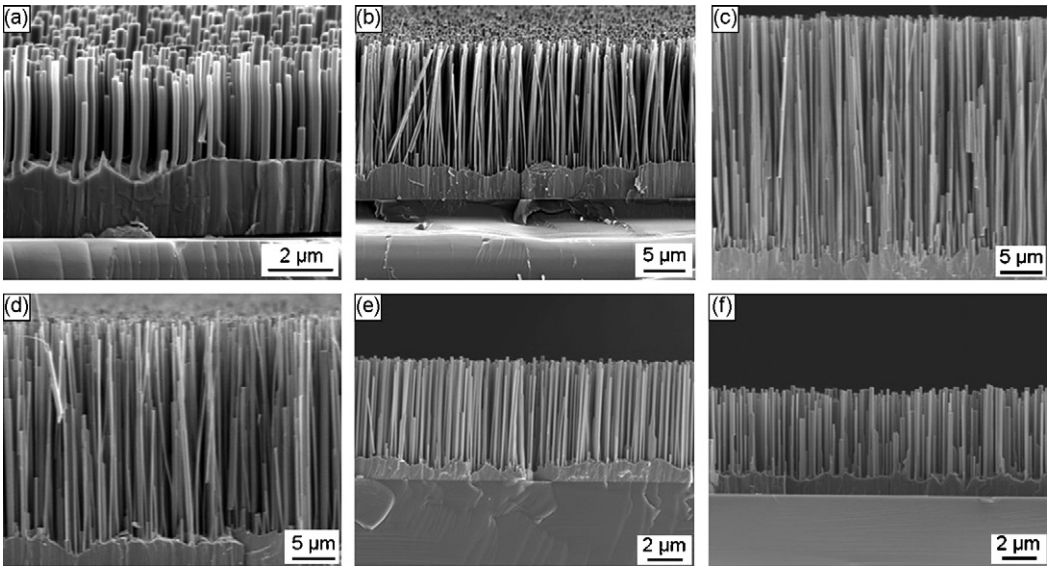

Fig. 7. FE-SEM cross section views of ZnO nanowires obtained in N_2 carrier gas: (a)–(d) are ZnO nanowire arrays deposited at 6, 10, 15 and 20 cm away from the source respectively under a flow rate of 5 sccm N_2 carrier gas. (e)–(f) are nanowire arrays deposited at 10 and 15 cm respectively under 20 sccm N_2.

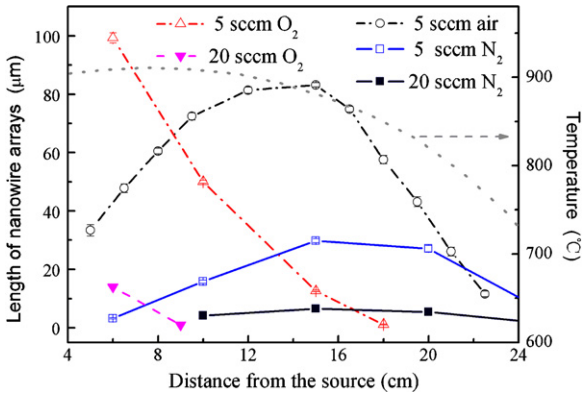

Fig. 8. The relationship between the length of the ZnO nanowire arrays and the deposition position under various carrier gases. The dot line shows the temperature gradient along the tube. The amount of O_2 in big quartz chamber plays a significant role in modulation of gaseous ZnO concentration along the slender tube. Temperature gradient plays minor role in length distribution.

3.4. Photoluminescence properties

Fig. 9 shows the room temperature PL spectra of as-synthesized nanowire arrays synthesized under different experimental conditions. All the samples show dominant UV emission located at about 387 nm, and weak, broad green band located at about 525 nm. The UV band is assigned to be near band edge (NBE) emission; the green band is commonly related to defect emission due to oxygen vacancies [36–38]. The appearance of visual band in PL spectrum indicates the presence of defects in ZnO [39]. Fig. 9a shows PL spectra of ZnO nanowire arrays obtained in different deposition zones. Sample A2 was deposited in the upstream, where O_2 was lack, according to our model. High oxygen vacancies concentration may exit. Thus, its green emission is relatively high (dash line shown in Fig. 9a). The intensity ratio of UV to visible emission (I_{UV}/I_{GR}) is 11. Sample A6 was obtained in the downstream, where O_2 was rich. Therefore, the defect emission is quite weak. A6 exhibits the largest UV emission efficiency ($I_{UV}/I_{GR} = 80$). Sample A4 is positioned in the midstream, where the local Zn and O_2 concentration are comparable. However, UV emission intensity as well as UV emission efficiency ($I_{UV}/I_{GR} = 10$) is the lowest among three samples. A possible reason is that the defect formation probability would increases with the rising of the growth rate [35].

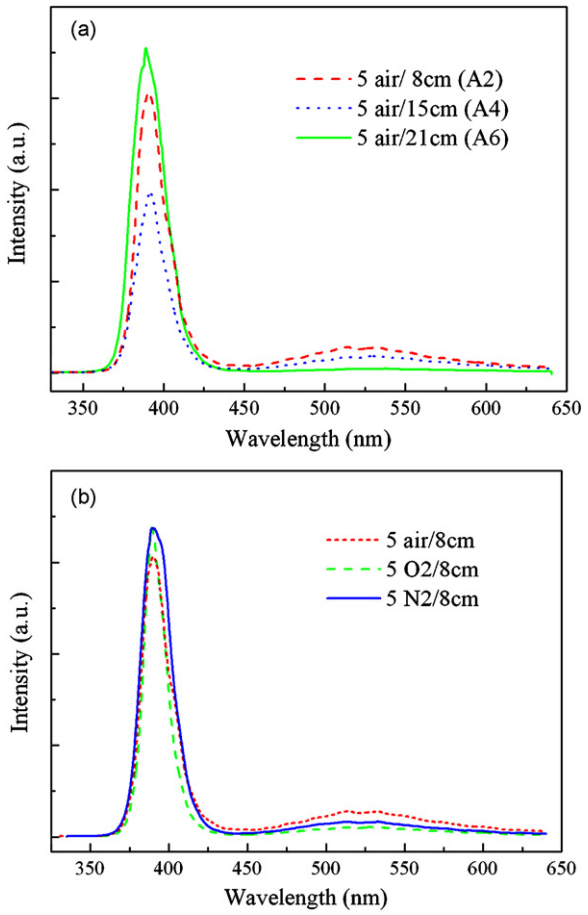

Fig. 9. Room temperature PL spectra (measured under the same excitation power) of as-synthesized ZnO nanowire arrays: (a) the effect of deposition zone on the PL properties of nanowire arrays, when 5 sccm air was used as carrier gas. (b) The influence of carrier gas on the PL spectra of ZnO nanowire arrays deposited at 8 cm away from the source.

Fig. 9b shows the influence of carrier gas on the PL spectra of nanowire arrays deposited in the upstream. Three samples exhibit similar PL spectra profiles. Sample deposited under O_2 atmosphere shows lowest defect emission ($I_{UV}/I_{GR} = 32$) due to high O_2 concentration. While sample deposited under N_2 atmosphere exhibits weaker defect emission ($I_{UV}/I_{GR} = 20$) than sample deposited under air atmosphere, which may arise from slow growth rate of nanowires. Based on our experimental data, we can conclude that sufficient O_2 atmosphere and slow growth rate would produce nanowire arrays with low defect concentration, which would benefit potential optoelectronic applications.

4. Conclusions

In summary, well-aligned ZnO nanowires were synthesized on thin ZnO coated Si wafers by VPT. The length of these nanowire arrays exhibits a quasi-continuous evolution along the axis of the small quartz tube. It was found that the type and flow rate of carrier gas have significant influences on the length distribution of nanowire arrays. ZnO nanowire arrays of arbitrary length (within the range) are expected to obtain by choosing proper carrier gas and deposition zone. The structural properties, growth mechanism, and optical properties were also discussed.

Acknowledgments

This work was supported by National Natural Science Foundation of China (No. 50672097) and Anhui Provincial Key Laboratory of Photonic Devices and Materials.

References

[1] Z.W. Pan, S.M. Mahurin, S. Dai, D.H. Lowndes, Nano Lett. 5 (2005) 723.
[2] L. Liao, H.B. Lu, J.C. Li, H. He, D.F. Wang, D.J. Fu, C. Liu, J. Phys. Chem. C 111 (2007) 1900.
[3] K. Hara, T. Horiguchi, T. Kinoshita, K. Sayama, H. Sugihara, H. Arakawa, Solar Energy Mater. Solar Cells 64 (2000) 115.
[4] H. Yumoto, T. Inoue, S.J. Li, T. Sako, K. Nishiyama, Thin Solid Films 345 (1999) 38.
[5] Z. Li, R.S. Yang, M. Yu, F. Bai, C. Li, Z.L. Wang, J. Phys. Chem. C 112 (2008) 20114.
[6] C.H. Ye, X.S. Fang, Y.F. Hao, X.M. Teng, L.D. Zhang, J. Phys. Chem. B 109 (2005) 19758.
[7] Z.L. Wang, J. Phys.: Condens. Matter 16 (2004) R829.
[8] H.J. Zhou, J. Fallert, J. Sartor, R.J.B. Dietz, C. Klingshirn, H. Kalt, D. Weissenberger, D. Gerthsen, H.B. Zeng, W.P. Cai, Appl. Phys. Lett. 92 (2008) 132112.
[9] Z. Zhang, J.B. Yi, J. Ding, L.M. Wong, H.L. Seng, S.J. Wang, J.G. Tao, G.P. Li, G.Z. Xing, T.C. Sum, C.H.A. Huan, T. Wu, J. Phys. Chem. C 112 (2008) 9579.
[10] L. Li, S.S. Pan, X.C. Dou, G.H. Li, L.D. Zhang, J. Phys. Chem. C 111 (2007) 7288.
[11] G.C. Yi, C.R. Wang, W.I. Park, Semicond. Sci. Technol. 20 (2005) S22.
[12] J.Y. Park, D.E. Song, S.S. Kim, Nanotechnology 19 (2008) 105503.
[13] M.H. Huang, S. Mao, H. Feick, H.Q. Yan, Y.Y. Wu, H. Kind, E. Weber, R. Russo, P.D. Yang, Science 292 (2001) 1897.
[14] C.S. Kee, D.K. Ko, J. Lee, J. Phys. D: Appl. Phys. 38 (2005) 3850.

[15] M. Riaz, A. Fulati, Q.X. Zhao, O. Nur, M. Willander, P. Klason, Nanotechnology 19 (2008) 415708.
[16] J.S. Jie, G.Z. Wang, Y.M. Chen, X.H. Han, Q.T. Wang, B. Xu, J.G. Hou, Appl. Phys. Lett. 86 (2005) 031909.
[17] L.S. Wang, X.Z. Zhang, S.Q. Zhao, G.Y. Zhou, Y.L. Zhou, J. Qi, J. Appl. Phys. Lett. 86 (2005) 024108.
[18] C. Li, G.J. Fang, Q. Fu, F.H. Su, G.H. Li, X.G. Wu, X.Z. Zhao, J. Cryst. Growth 292 (2006) 19.
[19] Y.K. Tseng, C.J. Huang, H.M. Cheng, I.N. Lin, K.S. Liu, I.C. Chen, Adv. Funct. Mater. 13 (2003) 811.
[20] C. Li, G.J. Fang, J. Li, L. Ai, B.Z. Dong, X.Z. Zhao, J. Phys. Chem. C 112 (2008) 990.
[21] F. Fang, D.X. Zhao, J.Y. Zhang, D.Z. Shen, Y.M. Lu, X.W. Fan, B.H. Li, X.H. Wang, Nanotechnology 18 (2007) 235604.
[22] X. Liao, X. Zhang, S. Li, Nanotechnology 19 (2008) 225303.
[23] P.D. Yang, H.Q. Yan, S. Mao, R. Russo, J. Johnson, R. Saykally, N. Morris, J. Pham, R.R. He, H.J. Choi, Adv. Funct. Mater. 12 (2002) 323.
[24] M.S. Gudiksen, J.F. Wang, C.M. Lieber, J. Phys. Chem. B 105 (2001) 4062.
[25] S.Y. Li, P. Lin, C.Y. Lee, Y. Tseng, J. Mater. Sci.: Mater. Electron. 15 (2004) 505.
[26] G. Meng, X.D. Fang, R.H. Tao, W.W. Dong, Z.H. Deng, S. Zhou, SPIE 7381 (2009) 73811Z.
[27] G. Meng, X.D. Fang, Y.K. Zhou, J.U. Seo, W.W. Dong, S. Hasegawa, H. Asahi, H. Tambo, M.G. Kong, L. Li, J. Alloys Compd. 491 (2010) 72.
[28] S.N. Cha, B.G. Song, J.E. Jang, J.E. Jung, I.T. Han, J.H. Ha, J.P. Hong, D.J. Kang, J.M. Kim, Nanotechnology 19 (2008) 235601.
[29] Y.F. Hao, G.W. Meng, Y. Zhou, M.G. Kong, Q. Wei, M. Ye, L.D. Zhang, Nanotechnology 17 (2006) 5006.
[30] M. Biswas, E. McGlynn, M.O. Henry, M. McCann, A. Rafferty, J. Appl. Phys. 105 (2009) 094306.
[31] P.C. Chang, Z.Y. Fan, D.W. Wang, W.Y. Tseng, W.A. Chiou, J. Hong, J.G. Lu, Chem. Mater. 16 (2004) 5133.
[32] H.W. Ra, K.S. Choi, Y.B. Hahn, Y.H. Im, J. Phys. Chem. C 112 (2008) 17926.
[33] C.Y. Geng, Y. Jiang, Y. Yao, X.M. Meng, J.A. Zapien, C.S. Lee, Y. Lifshitz, S.T. Lee, Adv. Funct. Mater. 14 (2004) 589.
[34] J.R. Welty, C.E. Wicks, R.E. Wilson, G.L. Rorrer, Fundamentals of Momentum, Heat and Mass Transfer, 4th edn, Jon Wiley & Sons, New York, 2001.
[35] E. Comini, Anal. Chim. Acta 568 (2006) 28.
[36] N.Y. Garces, L. Wang, L. Bai, N.C. Giles, L.E. Halliburton, G. Cantwell, Appl. Phys. Lett. 81 (2002) 622.
[37] S. Mandal, A. Dhar, S.K. Ray, J. Appl. Phys. 105 (2009) 033513.
[38] H.L. Yan, X.L. Zhong, J.B. Wang, G.J. Huang, S.L. Ding, G.C. Zhou, Y.C. Zhou, Appl. Phys. Lett. 90 (2007) 082503.
[39] J.B. Cui, M.A. Thomas, J. Appl. Phys. 106 (2009) 033518.